AIAA JOURNAL
Vol. 45, No. 1, January 2007

Influence of Stores on the Transonic Flutter of a Delta Wing Configuration

Hiroshi Terashima*
University of Tokyo, Tokyo 113-8656, Japan
and
Kozo Fujii†
Japan Aerospace Exploration Agency, Kanagawa 229-8510, Japan

DOI: 10.2514/1.24489

Transonic and supersonic flutter characteristics of a delta wing configuration with external stores were computationally simulated, and the aerodynamic influence of the stores on the flutter characteristics was investigated. Delta wings with one and two external stores were considered. Unsteady aerodynamics of the wing with external stores were evaluated using Navier–Stokes equations, and equations of motion based on a modal approach were applied to the structural dynamics. These equations were coupled using a subiteration approach. The computational results showed that the flutter dynamic pressures were reduced for a wide range of Mach numbers when the external stores were attached. The flutter dynamic pressures also decreased as the number of external stores increased. In the case of one external store, the aerodynamic influence of the store could be divided into two regions according to the Mach number. It was found that neglecting the aerodynamic influence of the store led to an overestimation of the flutter dynamic pressures in the supersonic flow region. In the case of two external stores, the aerodynamic influence of the stores on the flutter boundary appeared only at one supersonic Mach number, unlike the case of one external store. Additional flutter analysis using a different store size and unsteady aerodynamic analysis with forced oscillations indicated that the interference position of the shock wave generated ahead of the external store on the lower surface was a key factor in determining the flutter boundary, and the shock wave oscillation may have acted as a negative damping on the wing motion.

Nomenclature

b	=	semichord of wing root
C_p	=	pressure coefficient
c	=	wing root chord
$\hat{\boldsymbol{E}}, \hat{\boldsymbol{F}}, \hat{\boldsymbol{G}}$	=	inviscid flux vectors
f	=	flutter frequency
$\boldsymbol{f}_a$	=	aerodynamic forces vector
f_i	=	natural frequency of ith mode
$\boldsymbol{K}$	=	stiffness matrix
$\boldsymbol{M}$	=	mass matrix
M_i	=	generalized mass of ith mode
M_∞	=	freestream Mach number
$\hat{\boldsymbol{Q}}$	=	conservative variables vector
q_i	=	generalized displacement of ith mode
Re	=	Reynolds number
$\hat{\boldsymbol{S}}_v$	=	viscous flux vector
t	=	time
V_f	=	flutter velocity
V_{fsi}	=	flutter speed index, $V_{\text{fsi}} = V_f/2\pi f_2 b\sqrt{\mu}$
Δt	=	nondimensional time step size
μ	=	mass ratio
ξ, η, ζ	=	generalized coordinates
ϕ_i	=	eigenvector of ith mode
ω	=	circular frequency
ω_i	=	circular frequency of ith mode

Presented as Paper 2234 at the 34th AIAA Fluid Dynamics Conference and Exhibit, Portland, Oregon, 28 June–1 July 2004; received 7 April 2006; revision received 8 August 2006; accepted for publication 12 August 2006.

*Graduate Student, Department of Aeronautics and Astronautics; currently Research Scientist, The Institute of Physical and Chemical Research (RIKEN), 2-1 Hirosawa, Wako, Saitama 351-0198, Japan; htera@riken.jp. Member AIAA.

†Professor, Institute of Space and Astronautical Science, 3-1-1 Yoshinodai, Sagamihara, Kanagawa 229-8510, Japan. Fellow AIAA.

I. Introduction

REUSABLE launch vehicles are currently being investigated in various research laboratories with the aim of reducing rocket launching costs. Reusable launch vehicles, especially spaceplane types, usually have highly swept low-aspect-ratio wings, such as delta wings or arrow wings that reduce the wave drag. These vehicles experience a wide range of speeds, from subsonic to hypersonic, in their flight paths. During flight, the vehicles may be confronted with aeroelastic instability, such as flutter and buffeting, particularly in the transonic and low-supersonic flight regimes in which the corresponding dynamic pressure is large. Therefore, the transonic and supersonic flutter characteristics of low-aspect-ratio wing configurations are critical for the design and development of spaceplane-type vehicles.

According to earlier experimental research [1,2] on the flutter characteristics of simple delta wings, the flutter characteristics of simple delta wings were revealed to be similar to those of many other wing configurations. However, as pointed out by Doggett and Soistmann [3], there has been little research on the flutter characteristics of low-aspect-ratio wings compared with those of high-aspect-ratio wings for commercial airplanes.

It is known that the addition of external stores influences the flutter characteristics of the wing. The flutter characteristics of a clean wing are strongly dependent on the external stores mounted on the underside of the wing. Doggett and Ricketts [4] showed that an arrow wing with two nacelles has a deeper transonic bucket than a clean wing. They also reported that the geometries of the nacelles influence the flutter boundary. Their study with a flow-through nacelle and pencil nacelle indicated that the difference in flutter boundaries is attributed to the different nacelle aerodynamics, because the natural vibration characteristics of the two configurations were essentially the same. Durham et al. [5] showed that the flutter dynamic pressures for an arrow wing decrease as the number of engine nacelles

increases, especially in the transonic flow regime. Cole et al. [6] conducted a flutter test using a high-aspect-ratio wing with various combinations of external stores. In their experiment, to study the aerodynamic influence of the stores, they tested a fuel tank and pencil stores having the same mass and pitch and yaw inertia. Their results showed that the two store configurations exhibited different flutter boundaries, indicating that the aerodynamic influence of the stores on the flutter characteristics was significant. However, they concluded that the origin of this phenomenon is unknown. The experimental results of these groups showed that the addition of external stores plays an important role in the transonic flutter boundary and also indicated that the flowfield changed by the external stores may influence the flutter boundary. However, the aerodynamic influence of the store/nacelle on the flutter characteristics has not yet been fully clarified, and there has been no detailed experimental research into the effect of the flowfield on the flutter characteristics.

In numerical analysis, the aerodynamic influence of the stores is usually not included in numerical analysis of the flutter phenomenon, because the aerodynamic influence of the stores has been considered to be small and/or difficult to model, especially in the transonic flow regime [7,8]. Computational research in [9] showed that the inclusion of external store aerodynamics had a significant impact on the flutter characteristics. However, like the experimental studies, there was no discussion about the relationship between the flowfields and the flutter characteristics. In the past, there have been only a few studies using sophisticated computational fluid dynamics (CFD) techniques to estimate the aerodynamic influence of the store/nacelle. In the last decade, a fluid/structure coupling approach that solves the Euler/Navier–Stokes equations and the structural equations of motion has been developed and widely used for nonlinear aeroelastic analyses at transonic speeds [10–12].

The purpose of the present study is to investigate the aerodynamic influence of the stores on the flutter boundary of a low-aspect-ratio delta wing and to reveal the flowfields behind the flutter characteristics using the fluid/structure coupling approach. Navier–Stokes simulations are used to estimate the nonlinear aerodynamic behavior over a delta wing with external stores.

II. Numerical Procedure

A. Governing Equations and Aerodynamics Method

The governing equations used for the flowfields were unsteady three-dimensional compressible thin-layer Navier–Stokes equations in a generalized coordinate system, as follows:

$$\partial_t \hat{\boldsymbol{Q}} + \partial_\xi \hat{\boldsymbol{E}} + \partial_\eta \hat{\boldsymbol{F}} + \partial_\zeta \hat{\boldsymbol{G}} = Re^{-1} \partial_\zeta \hat{\boldsymbol{S}}_v \tag{1}$$

All variables were normalized by the combination of the freestream density, the freestream speed of sound, and the characteristic length, which was taken as the wing root chord in this study.

For the unsteady flow simulations, the three-point backward differencing with inner-iteration method [13] was used, and the second-order temporal accuracy was maintained. The lower-upper symmetric Gauss–Seidel (LU-SGS) algorithm [14] was used for the time integration. The numerical fluxes were estimated by the simple high-resolution upwind scheme (SHUS) [15], which is a family of advection upstream splitting method (AUSM)-type schemes. Higher-order spatial accuracy was obtained using monotone upstream-centered schemes for conservation laws (MUSCL) with primitive variable interpolation. The viscous terms were evaluated by central differencing, and the turbulent viscosity was modeled by the Baldwin–Lomax turbulence model [16].

The ratio of metrics to Jacobians was evaluated as an appropriate projected area of the cell faces, and the reciprocals of the Jacobians were evaluated as the cell volumes. The metrics and the Jacobians obtained by such an approach satisfied the geometric conservation law for moving and deformed grids [17].

At the inflow boundary, variables were specified as the freestream. At the subsonic outflow boundary, the pressure was fixed to the freestream value and other physical variables were extrapolated. For the supersonic outflow boundary, all physical variables were extrapolated. At the wall, the flow velocities match the wall velocities, which are equal to the grid speeds. The normal momentum equation, which includes the effect of wall acceleration on the pressure gradients, was used to define the pressure at the wall.

B. Governing Equations and Structural Dynamics Method

Second-order linear dynamic equilibrium equations were used for computing the structural deformation under aerodynamic forces. In this study, the governing equations were solved using a modal analysis approach, composing the solution with eigenvectors of the free vibration problem, as follows:

$$M_i \ddot{q}_i + M_i \omega_i^2 q_i = \phi_i^T \boldsymbol{f}_a, \qquad i = 1, \ldots, N \tag{2}$$

where N is the finite number of structural modes and

$$\omega_i^2 = \phi_i^T \boldsymbol{K} \phi_i, \qquad M_i = \phi_i^T \boldsymbol{M} \phi_i \tag{3}$$

The structural damping was not considered. Mass and stiffness matrices were derived using finite element modeling, and the eigenvectors and natural frequencies were calculated as an eigenvalue problem.

The time derivative operator was discretized by the three-point backward differencing with inner-iteration method in a similar manner as that for the aerodynamic equations. All physical variables were normalized by the same values as the aerodynamic equations.

C. Coupling Procedure

The fully implicit coupled approach proposed by Melville et al. [18] was applied to remove the sequencing effects between the aerodynamic and the structural equations.

The infinite plate spline (IPS) method [19] was used for interpolating the displacements from the structure grid points to the fluid grid points. The displacements obtained at each structural grid point were interpolated at the fluid grid points by the IPS method. The new geometry could then be obtained by adding the thickness in the normal direction to the deformed fluid grid points. The grid deformation approach developed by Melville et al. [18] was employed for a time-varying fluid grid system between the wing surface and the far field. The mapping algorithm presented by Bhardwaj et al. [20] was used to transfer the aerodynamic forces from the fluid grid points to the structure grid points. The aerodynamic forces were computed at each fluid grid point over the wing surface using the pressure, shear stress, and computational area.

D. Model Geometry

The geometric properties of the model configuration used in this study are presented in Fig. 1. These properties were determined based on several experimental models [3–5,21]. In particular, the wing model was the same as the experimental model of Doggett et al. [2] The wing model was a cropped delta wing with an aspect ratio of 0.54 and a leading-edge sweepback angle of 72 deg. The modified biconvex airfoil section had a thickness of 0.03, based on the chord.

The wing model was constructed of an 0.051-in.-thick aluminum alloy plate that was covered by balsa wood. In the present finite element analysis, the wing structure was assumed to be aluminum alloy plate for the sake of simplicity; that is, the balsa wood was not considered. Under this assumption, the weight of the wing model

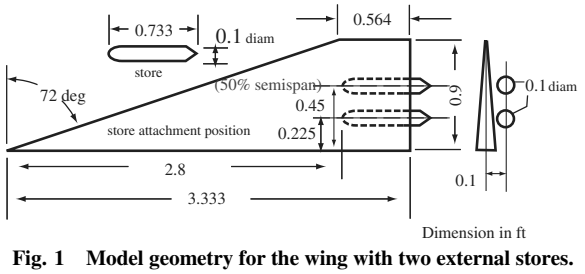

Fig. 1 Model geometry for the wing with two external stores.

Table 1 Mass properties for the wing and the external stores

	Density, lb/ft^3	Plate thickness, ft	mass, lb
Wing	167.931	0.00425	1.2518
Store (including pylon)	529.388	0.00443	0.5986

was about 0.53 times that of the experimental wing model. To match the mass ratio μ, which is an important nondimensional parameter for the flutter phenomena, the freestream density in the flow conditions was corrected to be small. Note that the mass ratio μ is defined as the ratio of the wing-panel mass and the fluid mass around the wing.

The external stores that simulated engine nacelles were mounted on the underside of the wing at about 25 and 50% of the wing semispan, as shown in Fig. 1. These stores were located at the rear of the wing in order to simulate the store location as seen in typical high-speed aircraft configurations, such as Concorde and spaceplanes. Each store provided a concentrated mass of about one-half of the wing-panel mass and was assumed to be formed only of steel plates. Mass properties for the wing and the external stores are given in Table 1.

E. Fluid Grid and Conditions

The overset grid approach was employed for a delta wing with one or two external stores, as shown in Fig. 2. The numbers of grid points were $273 \times 71 \times 61$ for the wing and $71 \times 67 \times 39$ for each store. The basic Navier–Stokes equations were modified for information exchanges between each grid zone. The interface method used in this study is called the fortified solution algorithm (FSA) [22], in which source terms are added to the basic Navier–Stokes equations as forcing terms to enforce the solutions on the other zones.

Flow conditions were taken directly from the flutter experiment of Doggett et al. [2] The freestream Mach number was set from 0.56 to 1.22, and the corresponding Reynolds number based on the wing root-chord length became 2.3×10^6 to 4.5×10^6. The wing was set at a 0 deg angle of attack. As described in the previous section, the freestream density was set to be smaller than under the experimental conditions, so that the mass ratio matched the experimental value.

F. Vibration Characteristics

The natural vibration frequencies and eigenvectors were computed. The delta wing, the external stores, and the pylon were modeled using quadrilateral shell elements. A typical finite element model used in this study is shown in Fig. 3.

The computed node lines and corresponding natural frequencies for the first three modes for the clean wing, the wing with one store, and the wing with two stores are presented in Fig. 4. Also included in Fig. 4 are the experimentally measured results for the clean wing. For all configurations, the first mode corresponded to the first bending mode, the second mode to the first torsional mode, and the third mode to the second torsional mode. Perspective views of the computed first three mode shapes of the wing with two stores are presented in Fig. 5.

The computed and measured nodal pattern for the clean wing were generally similar to the experimental measurements, as shown in Figs. 4a and 4b. The difference in the natural frequencies between the

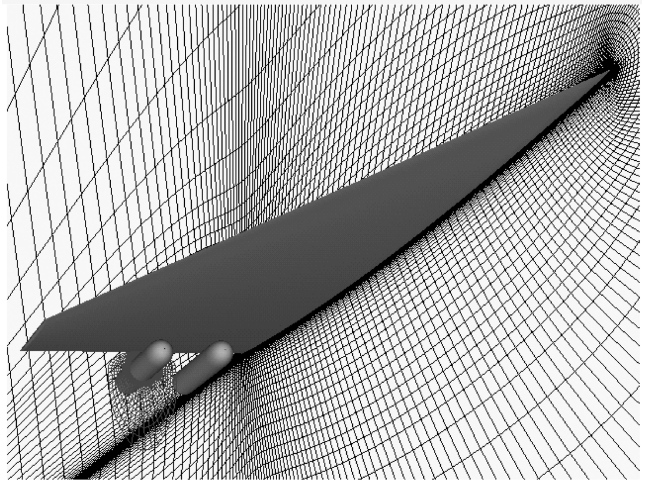

Fig. 2 Computational fluid grids for the wing with two external stores.

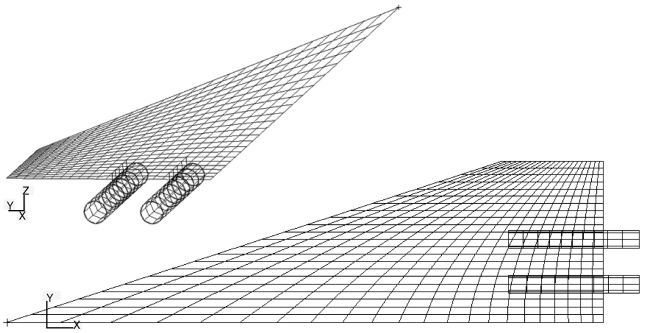

Fig. 3 Structural meshes of the delta wing with two external stores (560 elements).

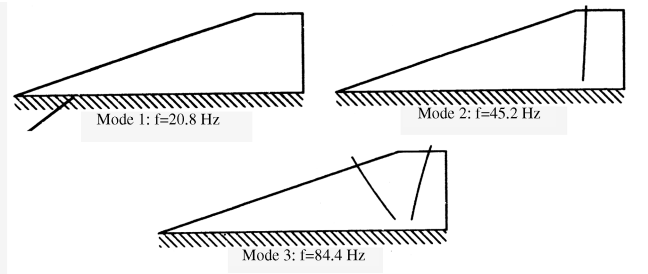

a) Experimental measurement for the clean wing model

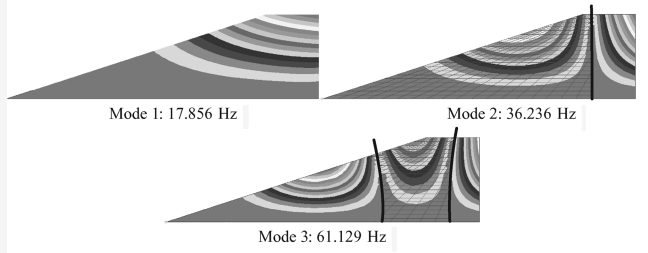

b) Clean wing model

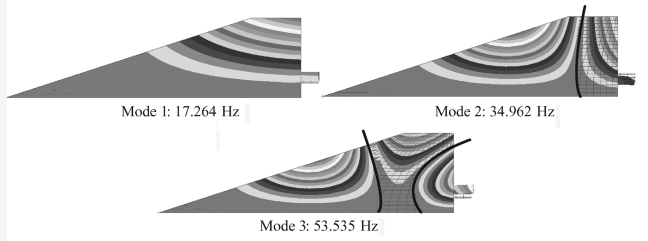

c) Wing with one store

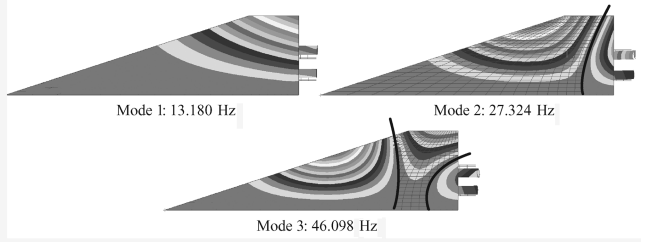

d) Wing with two stores

Fig. 4 Comparison of the node lines and natural frequencies for the first three modes.

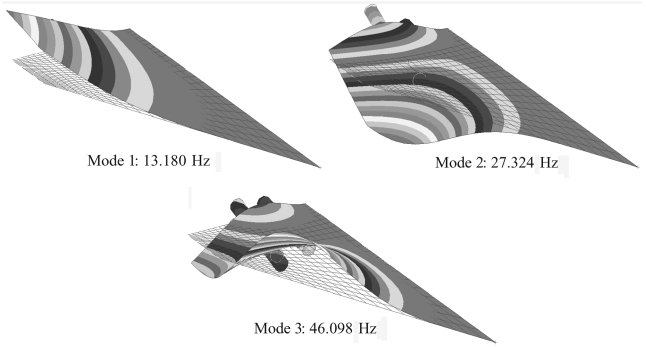

Fig. 5 Perspective views of the first three mode shapes and frequencies for the wing with two external stores.

measured and calculated results was due to the present structural finite element model, in which the mass and stiffness of the balsa wood was not accounted for. In fact, past analysis showed that use of an appropriate model led to agreement between the measured and calculated results [23].

As shown in Figs. 4c and 4d, the natural frequencies decreased with the weight of the external stores over all the modes. The node lines of the first torsional mode moved rearward of the wing as the number of external stores increased. The movement of the node lines of the first torsional mode leads to longitudinal instability and may cause a reduction of the flutter dynamic pressure; the numerical result of this is described in the next section.

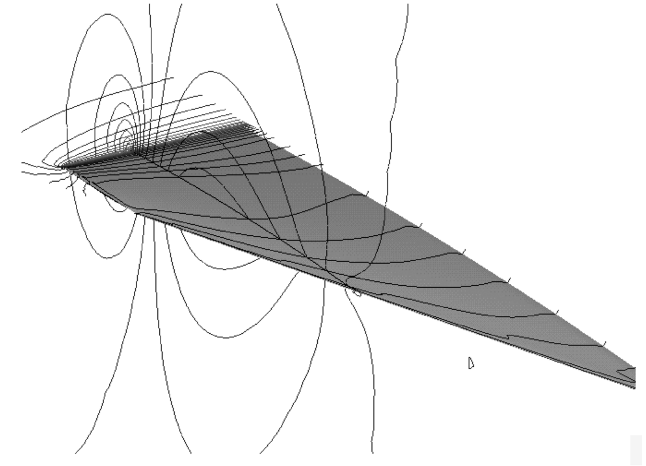

a) $M_\infty = 0.9$

b) $M_\infty = 1.1$

Fig. 6 Steady pressure contour plots over the wing surface and at about 65% spanwise section.

G. Flutter Data Processing

Time step size of the time integration was set to $\Delta t = 0.005$ in nondimensional time with three inner iterations. Preliminary numerical experiments indicated that three inner iterations were sufficient for estimating the time responses of the wing. All of the computations started with the corresponding steady-flow results. The first seven structural modes and the natural frequencies were considered in the present computations. For the initial conditions of the structural equations, a small perturbation, namely, 0.0001, for the first bending mode was applied to the wing. The freestream density was changed to vary the dynamic pressure.

III. Results and Discussions

A. Flutter Characteristics of the Clean Wing

Flutter characteristics of the clean cropped delta wing are discussed first, and the results are compared with the experiment of Doggett et al. [2] Figs. 6a and 6b show the steady-state pressure contour plots over the wing surface and at about 65% spanwise section at two Mach numbers, 0.9 and 1.1. A local shock wave was not observed over the wing surface at $M_\infty = 0.9$. At $M_\infty = 1.1$, a shock wave appeared at the trailing edge of the wing.

The flutter speed index V_{fsi} and flutter frequency ratio f/f_2 were computed and compared with the experimental data in Figs. 7a and 7b, respectively. The results for the pure delta wing configuration obtained from the experiment are also plotted in Fig. 7. Although the computed flutter speed index overpredicted the experimental flutter points by about 10% over all the Mach numbers, the trend of the computed flutter speed index was very similar to that found in the experiment. This overprediction was due to limitations of the present structural model, in which the wing was assumed to be constructed only of aluminum alloy plate for simplicity, although the actual plate was covered with balsa wood in the experiment. For this structural modeling, the computed second natural frequency used as the

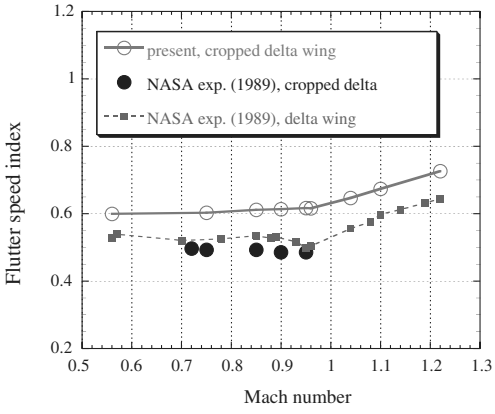

a) Flutter speed index

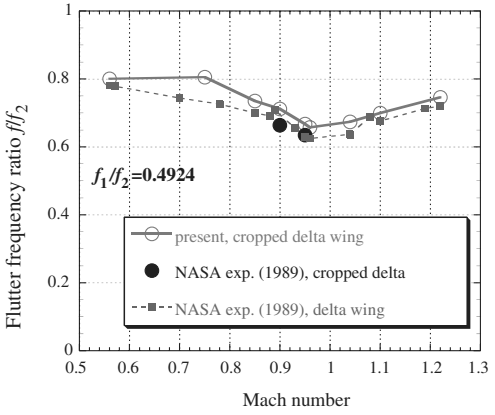

b) Flutter frequency ratio

Fig. 7 Flutter boundary for the clean wing configurations.

reference frequency of the flutter speed index was different from that measured in the experiment already shown in Figs. 4a and 4b. The difference between the computed and experimental frequencies was about 8%, which led to overprediction of the flutter boundary in the present computation.

The flutter speed index was almost constant through subsonic and transonic flow regions and increased as the flow became supersonic. The transonic dip, which is clearly observed for a typical high-aspect-ratio wing, was very shallow for the present cropped delta wing with a large sweepback angle. This is typical behavior of the flutter characteristics of low-aspect-ratio wings. The trend of the flutter frequency ratio also agreed well with the experiment. These results indicate that the present approach can accurately simulate the flutter characteristics for generic delta wings.

B. Flutter Characteristics of the Wing with One External Store

In this section, three cases are considered, and the influence of the external store on the flutter characteristics are examined. The three cases are as follows: 1) a clean wing; 2) a wing with a store, without considering the aerodynamic influence of the store; and 3) a wing with a store, with considering the aerodynamic influence of the store. In case 2, the effects of the external store (namely, the changes of mode shape and natural frequency) were considered in the structural analysis, but the fluid dynamic analysis did not include the external store. This means that flowfields around the wing were not altered at all by the external store. This corresponds to the conventional flutter analysis, in which the effect of the external store on the aerodynamics is not included. In case 3, the effects of the external store were considered both in the structural and fluid dynamic analyses. Flow conditions of these cases were the same as those of the clean wing case described in the previous section.

Figures 8a–8f show the steady C_p contour plots on the lower surface for the clean wing and the wing with one external store at $M_\infty = 0.75$, 0.90, 0.95, 1.04, 1.10, and 1.22, respectively. At $M_\infty = 0.75$, shown in Fig. 8a, the pressure distributions on the lower surface for the wing with one external store experienced almost no influence from the external store. At transonic $M_\infty = 0.90$ and $M_\infty = 0.95$, shown in Figs. 8b and 8c, expansion regions on the lower surface generated by the external store became larger than in the subsonic flow case. As the flow reached supersonic, the pressure distributions on the lower surface changed across the entire semispan due to the shock wave and the expansion wave generated by the external store, shown in Figs. 8d–8f. As also shown in Figs. 8d–8f, the interference position of the shock wave on the lower surface changed as the freestream Mach number increased.

Computed flutter characteristics for the clean wing; the wing with a store, without considering the aerodynamic influence of the store; and the wing with a store, with considering the aerodynamic influence of the store are presented in Figs. 9a and 9b as the variations

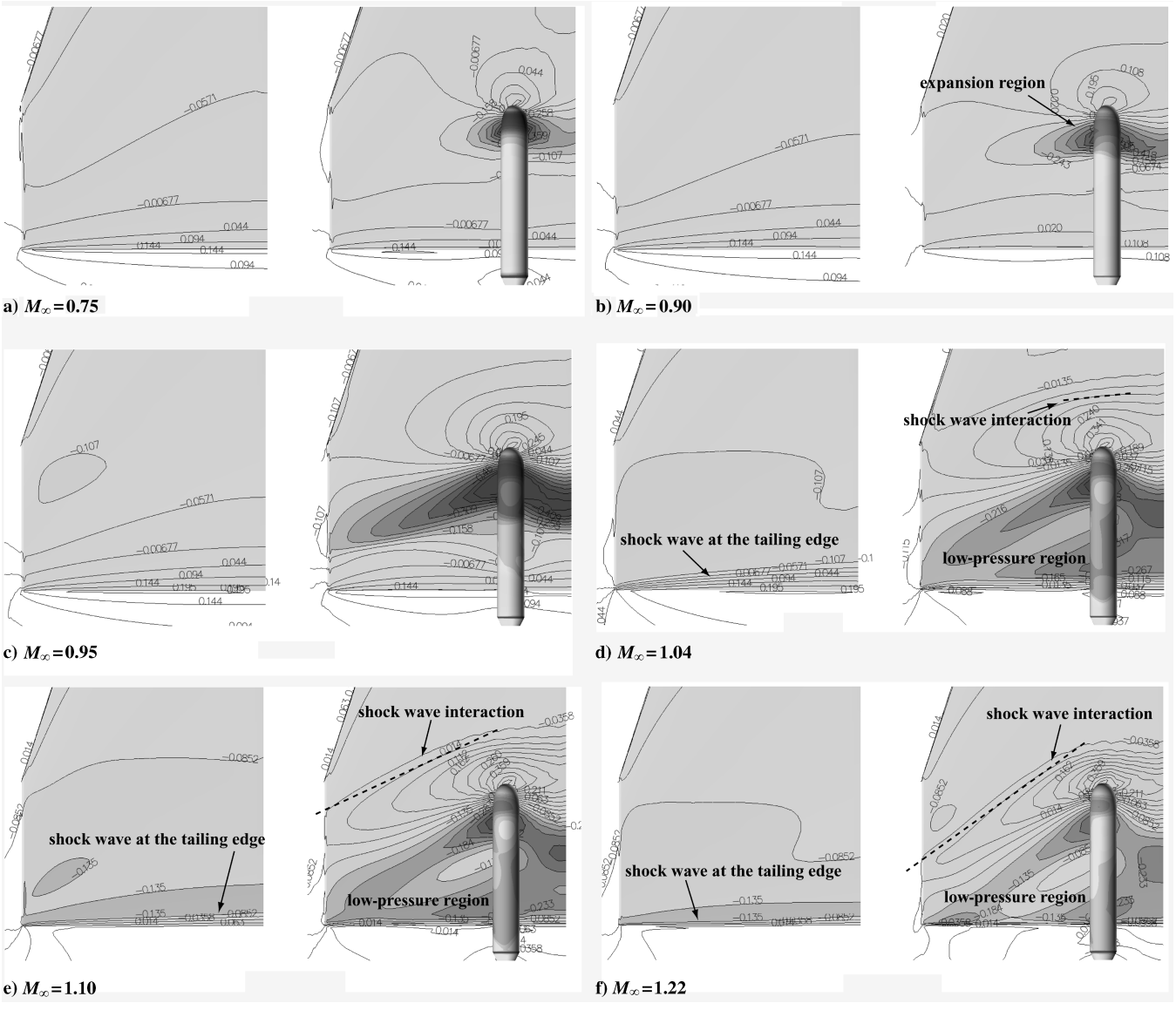

Fig. 8 Steady C_p contour plots on the lower surface for the clean wing (left) and the wing with one external store (right).

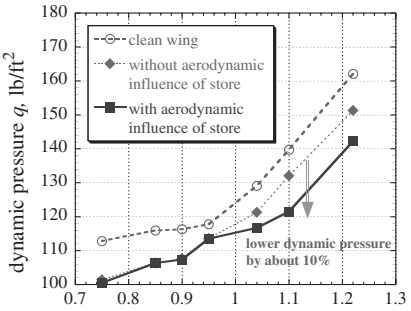

a) Dynamic pressure

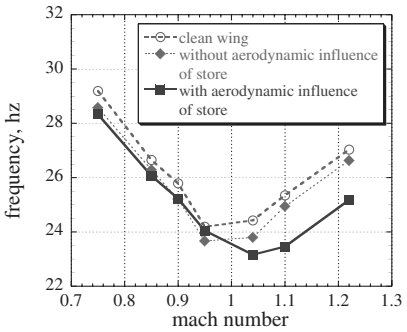

b) Frequency

Fig. 9 Flutter boundaries for the clean wing with one external store.

of flutter dynamic pressure and frequency with Mach number. The results for the clean wing shown in Figs. 9a and 9b correspond to those shown in Figs. 7a and 7b. The general trend of the flutter boundary of the wing both when considering the aerodynamic influence of the store and when not considering the aerodynamic influence of the store was similar to that of the clean wing. However, flutter dynamic pressures were lower than that of the clean wing over all Mach numbers. These results show that the addition of the external store at the rear of the wing had a destabilizing effect even when the aerodynamic influence of the store is not considered. The addition of the external store at the rear of the wing led to rearward movement of the center of gravity and resulted in increased longitudinal instability. This fact can also be confirmed from the movement of the node lines for the first torsional mode shown in Figs. 4b and 4c. As a result, flutter dynamic pressures of the wing with an external store decreased over all Mach numbers.

The aerodynamic influence of the store on the flutter boundary can be divided clearly into two regions according to the Mach number, as indicated in Figs. 9a and 9b. Below sonic flow, there was no significant change on the flutter boundary, because the existence of the external store hardly affected the pressure distributions on the lower surface, shown in Figs. 8a–8c. On the contrary, in the supersonic regions, flutter dynamic pressures of the wing with the store, when considering the aerodynamic influence of the store, became lower than when not considering the aerodynamic influence of the store. For example, the flutter dynamic pressure was almost 10% lower at $M_\infty = 1.1$, as indicated by the arrow in Fig. 9a. As already described in Figs. 8e and 8f, the pressure distributions over the lower surface were strongly influenced by the shock wave and the low-pressure regions generated by the external store. The resulting pressure distributions acting on the lower surface led to unstable motion of the wing, and the flutter dynamic pressure decreased mainly in the supersonic flow regions.

Flutter frequencies of the wing with the store, when considering the aerodynamic influence of the store, became smaller than those when not considering the aerodynamic influence of the store (Fig. 9b) as the flutter dynamic pressures in the supersonic flow regions decreased. This means that the first bending mode was slightly more dominant in the flutter phenomena due to the change in pressure distribution acting on the lower surface, which was caused by the external store. A previous study [24] reported that such a reduction of the flutter frequency due to the change in aerodynamics occurred with the occurrence of single-degree-of-freedom flutter at the transonic dip. In the present study, additional analysis was performed to investigate the unsteady aerodynamic behavior.

C. Flutter Characteristics of the Wing with Two External Stores

In this section, the wing with two external stores is considered, and the effect of the number of external stores on the flutter characteristics is examined. The same three cases as in the previous section are also considered, namely, 1) a clean wing; 2) a wing with stores, without considering the aerodynamic influence of the stores; and 3) a wing with stores, with considering the aerodynamic influence of the stores.

Figures 10a–10f show the steady C_p contour plots on the lower surface of the wing with two external stores. At $M_\infty = 0.75$, shown in Fig. 10a, the pressure distributions on the lower surface were not significantly influenced even when the second external store was added at the 50% semispan position. At $M_\infty = 0.90$ and $M_\infty = 0.95$, shown in Figs. 10b and 10c, the expansion region became larger than that of the wing with one external store, shown in Figs. 8b and 8c. The expansion region reached the wing tip. At supersonic flows, shown in Figs. 10d–10f, the pressure distributions were qualitatively the same as that of the wing with one external store. A shock wave appeared ahead of the external stores and interacted with the lower surface. The interference positions on the lower surface were shifted forward compared with the case of one external store, due to the addition of the outboard store, especially at the outboard region. Expansion waves were generated from the shoulders of the external stores, and a

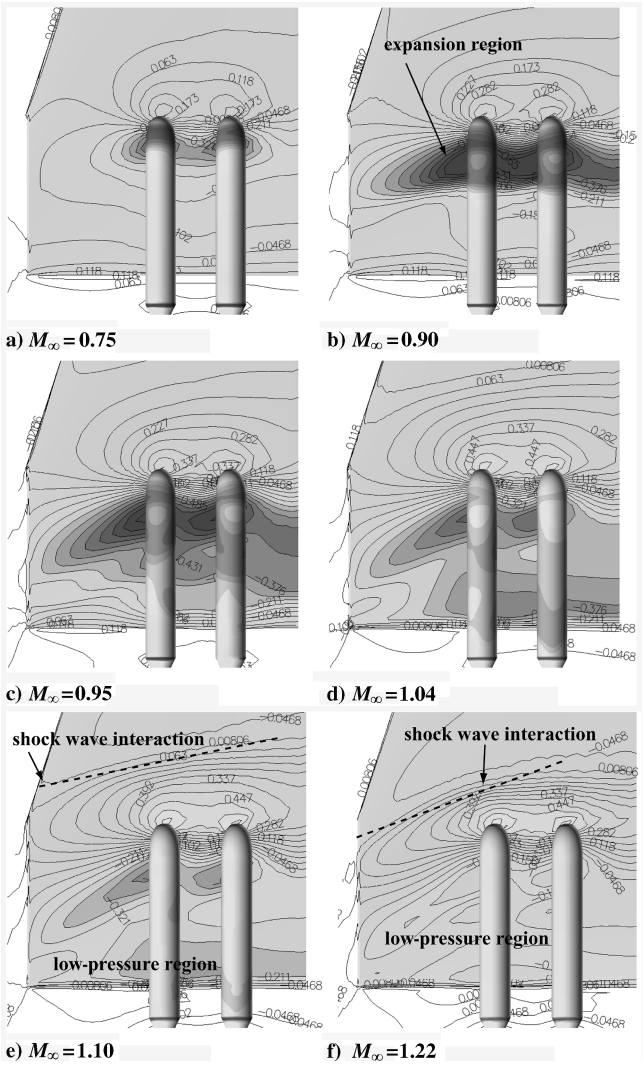

Fig. 10 Steady C_p contour plots on the lower surface of the wing with two external stores.

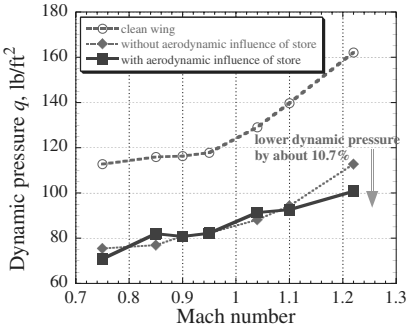

a) Dynamic pressure

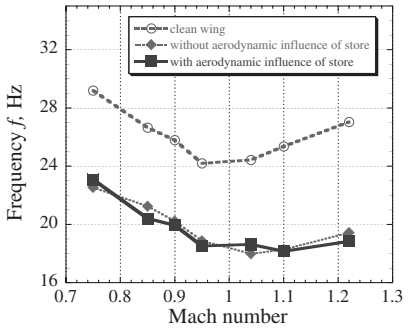

b) Frequency

Fig. 11 Flutter boundaries for the wing with two external stores.

region of lower pressure appeared over the rearward position of the lower surface. As the result, the C_p contour plots of the wing with two external stores at $M_\infty = 1.22$, shown in Fig. 10f, were similar to those of the wing with one external store at $M_\infty = 1.10$, shown in Fig. 8e.

Computed flutter characteristics for the clean wing; the wing with stores, without considering the aerodynamic influence of the stores; and the wing with stores, with considering the aerodynamic influence of the stores are shown in Figs. 11a and 11b. Flutter dynamic pressures of the wing with two external stores decreased considerably compared with those of the clean wing over all Mach numbers. The amount of reduction was larger than that of the wing with one external store, shown in Fig. 9a. This was because the node lines of the second mode, which was the first torsional mode, moves more rearward compared with the clean wing and the wing with one external store shown in Figs. 4b–4d. This rearward movement results in an increase of the longitudinal instability.

Figure 11a shows that the aerodynamic influence of the stores on the flutter boundary was not divided according to the Mach number like the flutter characteristics obtained for the wing with one external store. The differences between the wing with stores, both when considering the aerodynamic influence of the stores and when not considering the aerodynamic influence of the stores, can be seen only at $M_\infty = 1.22$, although the pressure distributions on the lower surface changed considerably due to the existence of the two external stores at other transonic Mach numbers, as shown in Figs. 10a–10f. These results indicate that the disturbed pressure distributions did not necessarily lead to a reduction of the flutter dynamic pressure.

According to the results obtained in the present study, the reduction of the flutter dynamic pressure caused by the aerodynamic influence of the store occur at $M_\infty = 1.1$ and 1.22 in the case of one external store and at $M_\infty = 1.22$ in the case of two external stores. The observation of these flowfields suggests that there were some similarities in the flowfields when the flutter characteristics changed. The key features were the shock wave ahead of the external store and the interference position on the lower surface. Namely, the shock wave interacted over the entire semispan, especially at the airfoil sections close to the wing tip, shown in Figs. 8e, 8f, and 10f. On the other hand, the flowfield at $M_\infty = 1.1$ with two external stores, when the flutter characteristics did not change, indicates that the shock wave did not interact with the airfoil sections close to the wing tip, shown in Fig. 10e. Furthermore, it is believed that the change in aerodynamics around the wing tip region had a larger effect on the wing motion than that around the other regions. Therefore, these results suggest that interference positions of the shock wave on the lower surface may be important in determining the flutter boundary for the cropped delta wing with external store configurations. In the next section, the importance of the shock wave on the flutter characteristics is discussed to verify this conclusion.

D. Results with Longer External Store and Behavior of Unsteady Aerodynamics

Two additional computations were performed to investigate the reduction of flutter dynamic pressure mentioned in the previous sections: 1) flutter analysis of a wing with a longer external store and 2) unsteady aerodynamic analysis using forced oscillations. Case 1 was used to investigate the influence of the shock wave location, and case 2 was used to examine the behavior of unsteady aerodynamic forces on the wing.

Figure 12 shows the comparison of model geometries between the original store configuration and the new longer one. The longer store was 1.5 times longer than the original store, and the nose of the longer store was located more forward than that of the original store. Although the lengths of the original and new stores was different, the total mass of each store was set to be the same, because the purpose of using the longer store was merely to change the interference position of the shock wave. Therefore, it was assumed that the wing with the longer store had the same vibration characteristics as the wing with the original store. In this section, the original store is called the shorter store, for comparison.

Figures 13a–13d show the steady C_p contour plots on the lower surface. The results for the shorter store are also presented to contrast the interference position of the shock wave. The shock wave interaction occurred much farther forward for the longer store than for the shorter store at both Mach numbers. The shock wave of the longer store did not interact with the tip region, unlike that of the shorter store.

Computed flutter characteristics of the wing with the longer store are shown in Figs. 14a and 14b. Also included in Figs. 14a and 14b are the results of the wing with the shorter store, both with and without the aerodynamic influence of the store already presented in Fig. 9. The flutter dynamic pressures of the wing with the longer store took similar values to those of the wing with the shorter store, without considering the aerodynamic influence of the store, at all Mach numbers, and the reduction of the flutter dynamic pressure in the supersonic flow region was not observed in the longer store. This trend can also be seen in the results of flutter frequencies in Fig. 14b. Although the shock wave of the longer store significantly influenced the lower surface, as shown in Fig. 13, the resulting flutter characteristics were generally similar to those of the wing with the shorter store without considering the aerodynamic influence of the store. These results indicate that the interference position of the shock wave played an important role in the prediction of flutter boundaries for cropped delta wings.

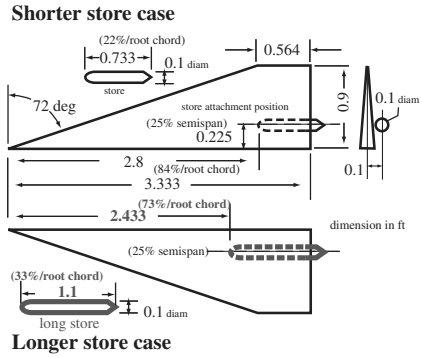

Fig. 12 Model geometry of the wing with the longer store compared with that of the wing with the shorter store.

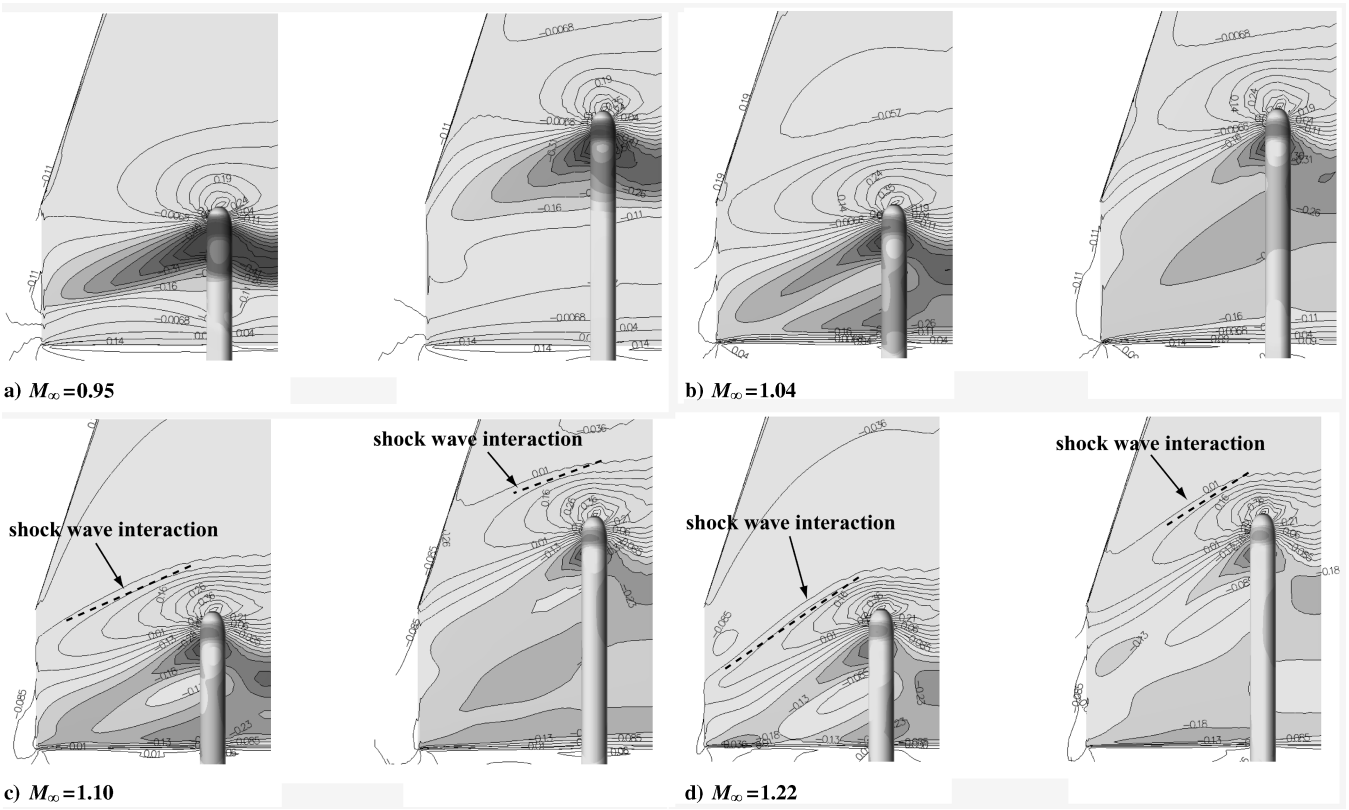

Fig. 13 Steady C_p contour plots on the lower surface for the wings with the shorter store (left) and the longer store (right).

In case 2 mentioned previously, the aerodynamic influence of the store was investigated for the wing with one external store under forced oscillation. As described previously, this analysis was carried out to examine the behavior of unsteady aerodynamics acting on the wing surface. The computed model was the wing with one external store, oscillating harmonically only in the second mode, which was the first torsion mode shown in Fig. 4c. Using the second mode, the motion of the wing with one external store corresponded to a forced pitching oscillation, and the nodal lines of second mode became a kind of pitching axis. The unsteady motion can be expressed as follows:

$$q_2 = \bar{q}_2 \sin(\omega t), \qquad \bar{q}_2 = 0.0001 \tag{4}$$

The computation using the forced oscillation was also performed for the wing with one external store without considering the aerodynamic influence of the store. Two Mach numbers, $M_\infty = 0.9$ and 1.1, were chosen as the flow condition. The flutter dynamic pressure was reduced due to the aerodynamic influence of the store at $M_\infty = 1.1$. The flutter frequency $f = 23.46$ Hz was selected as the pitching frequency in Eq. (4). The aerodynamic influence of the store did not appear in the flutter characteristics at $M_\infty = 0.9$. The flutter frequency $f = 25.23$ Hz at $M_\infty = 0.9$ was also used as the pitching frequency. The unsteady computations started from a converged steady-state solution obtained at a 0-deg angle of attack and five cycles of oscillation were calculated. The time variations of the computed surface C_p distributions were expressed in terms of the Fourier components in-phase and 90 deg out-of-phase, and the effects of unsteady aerodynamics on the wing surface are discussed next.

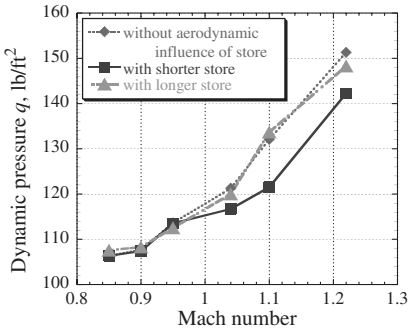

a) Dynamic pressure

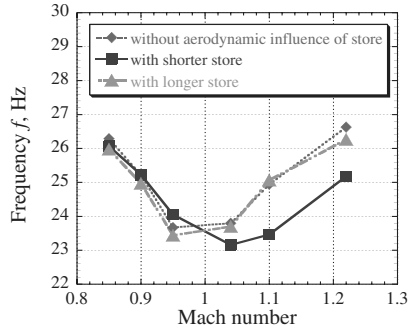

b) Frequency

Fig. 14 Flutter boundaries for the two configurations with one external store (shorter store and longer store) and for the wing without the aerodynamic influence of the store.

The computed real and imaginary parts of surface pressure coefficient distributions at $M_\infty = 1.1$, with and without the aerodynamic influence of the store, are shown in Figs. 15a and 15b. Figures 15a and 15b present the real and imaginary parts of surface C_p distributions at about 56.4 and 86.3% spanwise section, respectively. In Figs. 15a and 15b, there is clearly a peak, both in the real and imaginary parts, at both spanwise sections. Because such peaks were not observed in the results obtained when not considering the aerodynamic influence of the store, the shock wave motion over the lower surface seems to produce these peaks. The important feature is the negative peak of the imaginary part, which is the phase delay of the shock wave motion. It is well known that such a negative peak value of the imaginary part produces a certain amount of

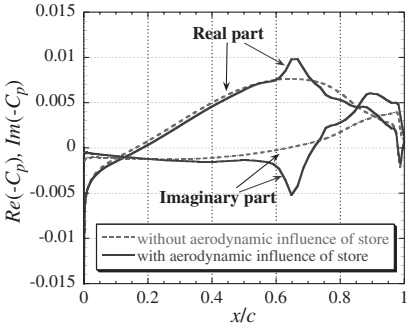

a) 56.4% spanwise section

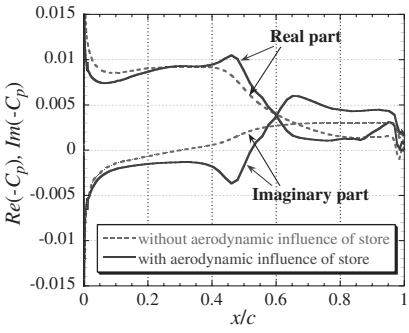

b) 86.3% spanwise section

Fig. 15 Unsteady pressure distributions on the lower surface with and without aerodynamic influence of the store at $M_\infty = 1.1$.

negative damping on the wing motion and leads to reduction of the flutter dynamic pressures [24]. The results for $M_\infty = 0.9$, as shown in Figs. 16a and 16b, show that the negative peak of the imaginary part did not appear at both spanwise section, unlike the results for $M_\infty = 1.1$, and there was almost no difference between the two results. Therefore, it is believed that the shock wave oscillation is a possible cause for the reduction of the flutter dynamic pressures in the supersonic flow region in this study.

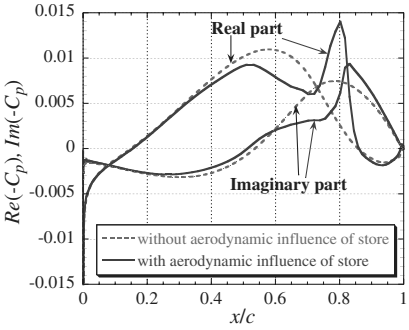

a) 56.4% spanwise section

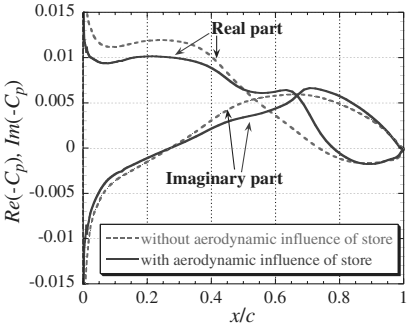

b) 86.3% spanwise section

Fig. 16 Unsteady pressure distribution on the lower surface with and without the aerodynamic influence of the store at $M_\infty = 0.9$.

IV. Conclusions

The aerodynamic influence of the stores on the transonic and supersonic flutter characteristics of a simple cropped delta wing was numerically investigated. The relationship between flutter characteristics and flowfield, which were changed by the external stores, was mainly discussed. Unsteady aerodynamics of the wing with external stores was evaluated using Navier–Stokes equations.

The addition of a rear-mounted store to the lower surface of a clean wing reduced the flutter dynamic pressure at all Mach numbers, due to the change of structural characteristics, even when the aerodynamic influence of the stores was not included. Increasing the number of external stores had a destabilizing effect on the flutter dynamic pressures.

In the case of the wing with one external store, the aerodynamic influence of the store was clearly divided into two regions according to the freestream Mach numbers. In the supersonic flow regions, it was found that neglecting the aerodynamic influence of the store led to overestimation of the flutter dynamic pressures. In the case of the wing with two external stores, the aerodynamic influence of the stores appeared only at supersonic $M_\infty = 1.22$.

Additional flutter analysis with a longer store suggested that the pressure distribution, especially the interference position of the shock wave on the lower surface, was a key factor in the flutter characteristics. Unsteady aerodynamic analysis with forced oscillation also indicated that the shock wave oscillation at that position was the origin of the negative damping of the wing motion. Therefore, it is concluded that the changes in flutter characteristics due to the aerodynamic influence of the store are caused by the shock wave interactions over the entire semispan for cropped delta wings.

References

[1] George, W. J., Jr., "Transonic Flutter Investigation of a 64° Delta Wing Constructed with Spars Along Constant-Percent Chord Lines and Streamwise Ribs," NACA RM L57G01, 1957.

[2] Doggett, R. V., Jr., Soistmann, D. L., Spain, C. V., Parker E. C., and Silva, W. A., "Experimental Transonic Flutter Characteristics of Two 72°-Sweep Delta-Wing Models," NASA TM 101659, Nov. 1989.

[3] Doggett, R. V., Jr., and Soistmann, D. L., "Low-Speed Flutter Characteristics of Some Simple Low-Aspect-Ratio Delta-Wing Models," *Journal of Aircraft*, Vol. 29, No. 2, Mar.–Apr. 1992, pp. 273–279.

[4] Doggett, R. V., Jr., and Ricketts, R. H., "Some Experimental and Theoretical Flutter Characteristics of an Arrow-Wing Configuration," AIAA Paper 77-422, 1977.

[5] Durham, M. H., Cole, S. R., Cazier, F. W., Jr., Keller, D. F., Parker E. C., and Wilkie, W. K., "Experimental Transonic Flutter Characteristics of Supersonic Cruise Configurations," AIAA Paper 90-0979-CP, 1990.

[6] Cole, S. R., Jose, A. R., Jr., and Nagaraja, K. S., "Flutter Study of an Advanced Composite Wing with External Stores," AIAA Paper 87-0880, 1987.

[7] Mykytow, W. J., "Recent Analysis Methods for Wing-Store Flutter," AGARD CP-162, 1974.

[8] Gern, F. H., Librescu, L., "Static and Dynamic Aeroelasticity of Advanced Aircraft Carrying External Stores," *AIAA Journal*, Vol. 36, No. 7, July 1998, pp. 1121–1129.

[9] Turner, C. D., "Effect of Store Aerodynamics on Wing/Store Flutter," *Journal of Aircraft*, Vol. 19, No. 7, July 1981, pp. 574–579.

[10] Gordnier R. E., and Merville, R. B., "Transonic Flutter Simulations Using an Implicit Aeroelastic Solver," *Journal of Aircraft*, Vol. 37, No. 5, Sept.–Oct. 2000, pp. 872–879.

[11] Potsdom M. A., and Guruswamy, G. P., "A Parallel Multiblock Mesh Movement Scheme for Complex Aeroelastic Applications," AIAA Paper 2001-0716, 2001.

[12] Yang, G., Obayashi S., and Nakamichi, J., "Aileron Buzz Simulation Using an Implicit Multiblock Aeroelastic Solver," *Journal of Aircraft*, Vol. 40, No. 3, May 2003, pp. 580–589.

[13] Chakraverthy, S. R., "Relaxation Methods for Unfactored Implicit Upwind Schemes," AIAA Paper 84-0165, 1984.

[14] Yoon S., and Jameson, A., "Lower-Upper Symmetric-Gauss-Seidel Method for the Euler and Navier–Stokes Equations," *AIAA Journal*, Vol. 26, No. 9, 1988, pp. 1025–1026.

[15] Shima E., and Jounouchi, T., "Role of CFD in Aeronautical Engineering (No. 14): AUSM Type Upwind Schemes," *Proceedings of the 14th NAL Symposium on Aircraft Computational Aerodynamics*, SP-34, National Aerospace Laboratory, Tokyo, Japan, Jan. 1997, pp. 7–12.

[16] Baldwin B. S., and Lomax, H., "Thin Layer Approximation and Algebraic Model for Separated Turbulent Flows," AIAA Paper 78-257, Jan. 1978.
[17] Tamura Y., and Fujii, K., "Conservation Law for Moving and Transformed Grids," AIAA Paper 93-3365-CP, 1993.
[18] Melville, R. B., Morton S. A., and Rizzetta, D. P., "Implementation of a Fully-Implicit, Aeroelastic Navier–Stokes Solver," AIAA Paper 97-2039, 1997.
[19] Harder R. L., and Desmarais, R. N., "Interpolation Using Surface Splines," *Journal of Aircraft*, Vol. 9, No. 2, pp. 189–191, 1972.
[20] Bhardwaj, M. K., Kapania, R. K., Eichenbach E., and Guruswamy, G. P., "Computational Fluid Dynamics/Computational Structural Dynamics Interaction Methodology for Aircraft Wings," *AIAA Journal*, Vol. 36, No. 12, Dec. 1998, pp. 2179–2186.
[21] Sandford, M. C., Rublin C. L., and Abel, I., "Transonic Flutter Study of a 50.5° Cropped-Delta Wing with Two Rearward-Mounted Nacelles," NASA TN D-7544, June 1974.
[22] Fujii, K., "Unified Zonal Method Based on the Fortified Solution Algorithm," *Journal of Computational Physics*, Vol. 118, 1995, pp. 92–108.
[23] Doggett, R. V., Jr., and Ricketts, R. H., "Effects of Angle of Attack and Vertical Fin on Transonic Flutter Characteristics of an Arrow-Wing Configuration," NASA TN D-7544, June 1974.
[24] Isogai, K., "Numerical Study of Transonic Flutter of a Two-Dimensional Airfoil," National Aerospace Laboratory, Rept. TR-617T, July 1980.

E. Livne
Associate Editor